Scripta Materialia 147 (2018) 59–63

Contents lists available at ScienceDirect

Scripta Materialia

journal homepage: www.elsevier.com/locate/scriptamat

Regular article

Microstructural degradation of polycrystalline superalloys from oxidized carbides and implications on crack initiation

Paraskevas Kontis [a,*], David M. Collins [b], Angus J. Wilkinson [c], Roger C. Reed [c], Dierk Raabe [a], Baptiste Gault [a]

[a] Max-Planck-Institut für Eisenforschung, Max-Planck-Str. 1, 40237 Düsseldorf, Germany
[b] School of Metallurgy and Materials, University of Birmingham, Edgbaston B15 2TT, UK
[c] Department of Materials, University of Oxford, Parks Road, OX1 3PH Oxford, UK

ARTICLE INFO

Article history:
Received 17 November 2017
Received in revised form 24 December 2017
Accepted 26 December 2017
Available online xxxx

Keywords:
Oxidized carbides
Recrystallization
Atom probe tomography
γ′ Dissolution
Partial dislocation

ABSTRACT

Surface connected carbides in a polycrystalline superalloy oxidized at 750 °C in air were studied as potential crack initiation sites. Lattice rotations measured in the γ/γ′ grains using high-resolution electron backscatter diffraction enabled investigation of the plastic deformation induced solely by the oxidation of carbides. Dislocations were found to enhance γ′ precipitate dissolution kinetics, resulting in soft recrystallized regions in the vicinity of the oxidized carbide with substantial compositional variation compared to the original γ/γ′ microstructure. Ramifications of such deleterious oxidized carbides alongside soft recrystallized regions on the crack initiation life in superalloys are discussed.

MC-type carbides are known to serve as crack initiation sites under fatigue conditions at elevated temperatures in nickel-based superalloys by acting as stress concentration sites [1]. These inherently brittle particles cannot easily accommodate plastic deformation when subjected to high stresses, instead failing through fracture or decohesion from the γ/γ′ microstructure. Micro-cracks originating from these loci may subsequently propagate [2]. When tested under complex stress and temperature cycles, the cracks may instead initiate in regions close to a free surface, originating from an oxidized MC carbide, and subsequently propagate within the bulk [3,4]. The products from the oxidation of the MC carbides result in their volume expansion, subsequently generating significant local plastic deformation [5]. Nevertheless, the exact mechanism for crack initiation by oxidized carbides is not well understood. For instance, it is not clear to what extent the localised plastic deformation occurs and whether the composition of the γ/γ′ microstructure can be potentially altered.

Advanced characterisation techniques that offer spatially resolved quantification of deformation and composition now enable the mechanisms governing oxidized carbide failure to be investigated. Specifically, the combination of high angular resolution electron backscatter diffraction (HR-EBSD) permits characterisation of plasticity mechanisms and can be linked to composition measurements made using atom probe tomography (APT). From HR-EBSD, plastic deformation is inferred by quantifying the geometrically necessary dislocation (GND) density and distribution [6], based upon measurements of the lattice curvature and subsequent analysis of the Nye tensor [7]. This experimental method has previously been applied to superalloys to study the accumulation of GND fields near grain boundaries and non-metallic inclusions [8,9]. APT analysis of oxide particles and oxide scales from superalloys, oxide dispersion-strengthened ferritic alloys and steels have been successfully characterised giving accurate chemical composition data [10–15].

In this study, a polycrystalline superalloy IN792, commonly used in industrial gas turbines, was investigated. The chemical composition of the alloy is Ni-13.9Cr-8.8Co-1.1Mo-1.3W-7.6Al-4.9Ti-1.3Ta-0.4C-0.1B-0.012Zr (at.%). The carbon content was measured using a LECO CS444 analyser and for the other elements by inductively coupled plasma OES. Conventionally cast round bars with 20 mm diameter were supplied by Howmet. The as-cast bars were hot isostatically pressed (HIP) at 1195 °C and 150 MPa for 2 h followed by solution heat treatment at 1121 °C for 2 h. The final stage of ageing was conducted at 850 °C for 24 h. Specimens were ground and polished with abrasive media to a 1 μm (diamond suspension) finish (the surface roughness was not measured after the polishing stage) from a fully heat-treated bar and were isothermally and statically exposed at 750 °C for 50 h under no external mechanical loading.

A dual column scanning electron microscope (SEM) and focused ion beam (FIB) Zeiss NVision 40 was used for surface observations, and HR-EBSD provided details on the plasticity mechanism in the vicinity of an

* Corresponding author.
E-mail address: p.kontis@mpie.de (P. Kontis).

https://doi.org/10.1016/j.scriptamat.2017.12.028
1359-6462/

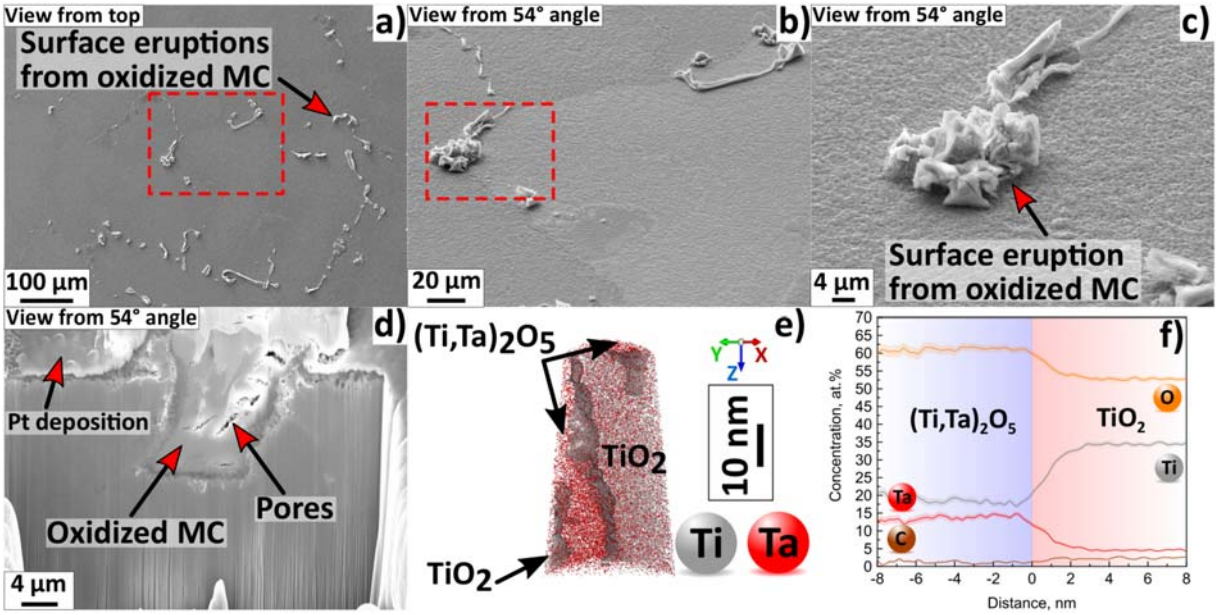

Fig. 1. Secondary SEM micrographs showing: a) top view of surface eruptions from oxidized MC carbides. b) Intergranular and intragranular oxidized MC carbides as denoted by the red dashed box in Fig. 1a shown with the sample tilted 54° normal to the electron beam. c) Detail of surface eruption from the intergranular oxidized MC carbide denoted by the red dashed box in Fig. 1b. d) FIB section normal to the sample surface showing the oxidized MC carbide from Fig. 1c within the bulk and the formation of pores, e) APT reconstruction from an oxidized MC carbide showing with an iso-concentration surface at 23.0 at.% Ti, $TiO_2/(Ti,Ta)_2O_5$ interfaces and f) concentration profile across the $TiO_2/(Ti,Ta)_2O_5$ interface. Error bars are shown as lines filled with colour and correspond to the 2σ counting error. (For interpretation of the references to colour in this figure legend, the reader is referred to the web version of this article.)

oxidized MC carbide. A nickel layer was electrochemically deposited on the surface prior to preparation. The cross-section of the statically-exposed specimen was polished to a 0.04 µm colloidal silica finish. A JEOL 6500F field emission gun SEM operated at 20 kV and a current of ~14 nA, equipped with a TSL Digiview II Peltier-cooled charge coupled device was used. From a region-of-interest, a 14 × 10 $µm^2$ EBSD map was collected with 0.05 µm step size. EBSD patterns were recorded at full resolution (1000 × 1000 pixel) with 0.5 second exposure. The GND density was estimated using an in-house analysis method to quantify lattice curvature [6]. The areas of the GND map blanked are from oxidized and non-oxidized MC carbides for which the exact crystallographic information is unknown.

APT was used to investigate chemical variations between recrystallized grains and the deformed γ/γ′ microstructure. Site-specific specimens were prepared from both regions, the MC carbide before and after oxidation, using a dual column SEM-FIB FEI Helios 600 following procedures described in Ref. [16], and analysed on a Cameca LEAP 5000 HR operated at a base temperature of 60 K in laser pulsing mode at 125 kHz, with 0.45 pJ pulse energy.

Fig. 1a shows surface eruptions caused by the oxidation of MC carbides. Both inter- and intragranular carbides located close or connected to the surface oxidize, as shown in Fig. 1b–c. Similar oxidized carbides in statically exposed samples have previously been reported [8,17,18]. A FIB cross-section of the intergranular oxidized carbide is shown in Fig. 1d, in which the formation of pores due to the oxidation of the carbide is apparent. Pores are likely forming due to the outward formation of the oxide products towards the free surface. Pores formed after only 50 h of static exposure at 750 °C in absence of external applied stress. Pores are known to serve as stress concentration sites where cracks can initiate in superalloys [19]. Thus, our observations give a first strong indication that cracks can primarily initiate within or in the vicinity of oxidized MC carbides.

Oxidation of the MC carbide was confirmed by APT, and Table 1 provides compositions of a MC carbide after heat treatment and one after isothermal static exposure in air at 750 °C for 50 h. In the former, the MC carbide is Ti/Ta-rich, with low concentration of molybdenum and tungsten. After thermal exposure, the chemistry of the MC carbide was altered substantially. In Fig. 1e, APT of an oxidized MC carbide shows two regions with different concentrations of Ti, Ta and O that likely correspond to TiO_2 and $(Ti,Ta)_2O_5$. An elemental composition profile as a function of the distance from the $TiO_2/(Ti,Ta)_2O_5$ interface (i.e. proxigram [20]) is presented in Fig. 1f and the compositions is in Table 1. The oxygen concentration is lower than the expected stoichiometry, which can be ascribed either to a metastable state of the oxide or to an underestimation due to loss in detection [21,22]. Interestingly, the carbon content dramatically decreased from 47.40 at.% to only 2.3 at.% in the TiO_2 and 1.1 at.% in $(Ti,Ta)_2O_5$, confirming oxidation. It is believed that carbon during the oxidation of the carbides contributes towards the formation of CO or CO_2 gas.

Substantial volume expansion due to the oxidation of MC carbides can result in localised plastic deformation [3,18], as confirmed here by HR-EBSD. A backscattered-electron micrograph near a partially oxidized MC carbide is shown in Fig. 2a. The carbide is not entirely oxidized as observed by the distinct changes in contrast within the particle. The part of the carbide furthest from the surface appears unaffected. Recrystallization was observed around the oxidized carbide, as evidenced by the EBSD inverse pole figure map shown in Fig. 2b. During exposure at elevated temperatures, and below the protective oxide scale at the surface, a γ′ denuded zone forms, where recrystallization is often observed [10]. However, in our case, recrystallization is only present close to the

Table 1
Summary of chemical compositions of the MC carbide after full heat treatment and after isothermal exposure in air at 750 °C for 50 h as measured by atom probe tomography (at.%).

	C	Ni	Cr	Al	Ti	Ta	Mo	W	O
MC	47.4 ± 0.02	0.0	0.5 ± 0.01	0.0	30.0 ± 0.04	18.5 ± 0.03	1.7 ± 0.01	1.6 ± 0.01	0.00
MC/TiO_2	2.3 ± 0.01	1.7 ± 0.08	1.0 ± 0.06	1.0 ± 0.07	34.1 ± 0.09	4.7 ± 0.06	0.0	1.2 ± 0.03	52.9 ± 0.45
$MC/(Ti,Ta)_2O_5$	1.1 ± 0.01	0.4 ± 0.11	0.3 ± 0.06	0.4 ± 0.05	18.5 ± 0.07	13.7 ± 0.05	0.0	3.5 ± 0.01	61.3 ± 0.17